Received 15 March 2022; revised 17 June 2022 and 10 October 2022; accepted 10 October 2022. Date of publication 19 October 2022; date of current version 13 December 2022. The review of this paper was arranged by Editor Alberto Mazzoni.

Digital Object Identifier 10.1109/OJEMB.2022.3215726

A Biorealistic Computational Model Unfolds Human-Like Compliant Properties for Control of Hand Prosthesis

ZHUOZHI ZHANG [1], JIE ZHANG [1], QI LUO[1], CHIH-HONG CHOU [1,2], ANRAN XIE[1], CHUANXIN M. NIU [1,2] (Member, IEEE), MANZHAO HAO [1,2], AND NING LAN [1,2] (Senior Member, IEEE)

[1]Laboratory of Neurorehabilitation Engineering, School of Biomedical Engineering, Shanghai Jiao Tong University, Shanghai 200240, China
[2]Institute of Medical Robotics, Shanghai Jiao Tong University, Shanghai 200240, China

CORRESPONDING AUTHOR: NING LAN (e-mail: ninglan@sjtu.edu.cn)

This work was supported in part by grants from the National Key R&D Program of China under Grant 2017YFA0701104, in part by the National Natural Science Foundation of China under Grant 81630050, and in part by the Science and Technology Commission of Shanghai Municipality under Grant 20DZ2220400.
This article has supplementary downloadable material available at https://doi.org/10.1109/OJEMB.2022.3215726, provided by the authors.

ABSTRACT *Objective:* Human neuromuscular reflex control provides a biological model for a compliant hand prosthesis. Here we present a computational approach to understanding the emerging human-like compliance, force and position control, and stiffness adaptation in a prosthetic hand with a replica of human neuromuscular reflex. *Methods:* A virtual twin of prosthetic hand was constructed in the MuJoCo environment with a tendon-driven anthropomorphic hand structure. Biorealistic mathematic models of muscle, spindle, spiking-neurons and monosynaptic reflex were implemented in neuromorphic chips to drive the virtual hand for real-time control. *Results:* Simulation showed that the virtual hand acquired human-like ability to control fingertip position, force and stiffness for grasp, as well as the capacity to interact with soft objects by adaptively adjusting hand stiffness. *Conclusion:* The biorealistic neuromorphic reflex model restores human-like neuromuscular properties for hand prosthesis to interact with soft objects.

INDEX TERMS Compliant control, computational modeling, neuromuscular reflex, prosthetic hand, stiffness adaptation.

IMPACT STATEMENT Results elucidate the emerging human-like properties of adaptive compliant control endowed with the biorealistic neuromorphic reflex model for next-generation hand prosthesis.

I. INTRODUCTION

In spite of remarkable advances in the design, manufacture and control of myoelectric bionic hand prosthesis [1], [2], [3], [4], performance of these devices is acceptable at best when compared to the dexterity of human hand [5], [6], [7]. Research on restoring the functions of lost limbs in past decades has motivated several generations of neural prosthesis [2], [8], [9], [10]. A primary challenge for existing bionic hand prosthesis is to execute precision tasks, such as grasping deformable or brittle objects. A major limitation of present prosthetic hands is that its motor control does not behave similarly as human sensorimotor control. This may lead to frustration in amputees who could not adapt to the alien behaviors of the prosthetic hand, therefore, hesitating using it to perform activities in daily living [7], [11], [12].

The importance of compliant control has been recognized in robotics. Recently, soft robotic hands with pneumatic actuation have demonstrated compliant property and robust grasp of soft objects [13], [14], [15]. Their compliance is derived from pneumatic actuation, soft materials and/or flexible structures. But the range of compliance in soft robotic hands may still be limited compared to that of human hand driven by muscles [16], [17].

Alternatively, we developed a biorealistic approach for hand prosthesis leveraging computational models to restore human-like neuromuscular control [18]. Real-time

reanimation of human neuromuscular reflex for prosthetic hand was achieved with neuromorphic models of biologically realistic elements [18], [19], [20], [21], [22], [23]. Functional benefits have been demonstrated in tests with amputees-in-the-loop controlling the biorealistic prosthesis. The capacity of finger force control was found comparable to that of an intact hand finger, but significantly better than that of a conventional prosthetic controller [24]. The ability to complete delicate tasks was revealed in tests to grasp slipping or brittle objects, such as picking up golf balls or potato chips [25]. However, this prototype of biorealistic hand still lacked antagonistic muscle control of finger movements. Specifically, its biorealistic properties were not fully understood with regard to the origin of compliance and the maneuverability of hand stiffness via myoelectrical signals from amputees.

The objective of this study was to unveil the underlying human-like compliant properties embedded in the biorealistic hand prosthesis. A virtual twin of the prosthetic hand with antagonistic muscle control for finger flexion and extension movements was constructed for real-time simulation. The main goal was to elucidate the adaptive mechanism of prosthetic hand stiffness during interacting with a soft object. We hypothesized that the biorealistic modelling approach can restore human-like compliant properties for hand prosthesis. Tests unveiled that the neuromorphic-based computational model displayed similar behaviors of stiffness regulation and the capacity of force control as those of humans qualitatively. Results indicated that the biorealistic controller acquired a wide range of stiffness/force control ability, as well as adaptive adjustment of hand stiffness when interacting with a soft object. The similarity with human sensorimotor control may lead to a superior neural compatibility for amputees to better control the biorealistic hand prosthesis [24], [25]. Preliminary result was presented in a conference proceeding [26].

II. RESULTS

A virtual twin of the biorealistic hand prosthesis was developed in the MuJoCo environment with tendon-driven actuation, fingertip tactile sensors and neuromorphic reflex model (for details, see Fig. 5(b) in Methods). The virtual twin was integrated with a pair of neuromorphic antagonistic muscles emulating neuromuscular reflex control [23] and a sensory feedback system via electrically evoked tactile sensation (ETS) [27]. To simplify the control issue of whole virtual hand, we investigated the control problem of a prosthetic index finger by a pair of antagonistic muscles. A comprehensive evaluation on virtual hand properties was conducted to reveal its human-like behaviors with a qualitative comparison to the corresponding features of human neuromuscular reflex control.

A. CONTROL OF FINGERTIP FORCE AND POSITION

Fig. 1(a) presents an overview of prosthetic control system. α motor commands activated a pair of antagonistic muscles with neuromorphic reflex model controlling the index finger. Muscle outputs drove two motors pulling the index finger of the virtual hand.

Central to control the system was the Hill's muscle model in Fig. 1(b). The α motor command was converted to an activation signal through a motoneuron pool (MP) and a twitch model (TM). The latter acted as a low-pass filter and converted a spiking activation to a muscle twitch signal to drive the Hill-type muscle. Muscle force was generated through an activation-contraction process [28], [29], [30], [31], [32], in which three factors determined force generation, i.e., activation factor, fascicle length factor and contraction velocity factor [29]. The most important element of muscle force production was the modulation by length-tension effect in Fig. 1(c) [29], [31]. It was described by a parabolic shape with a positive stiffness segment and a plateau followed by a negative stiffness range [29]. In this study, the range of muscle fascicle length (L_{ce}) was set to operate in the positive stiffness part of length-tension property to assure stability during external perturbations. Therefore, L_{ce} range for flexor was chosen between $0.80 \sim 0.95\ L_o$ and for extensor was between $0.75 \sim 0.90\ L_o$. The parallel, serial and tendon elastic elements worked together to transform musculotendon length (L_{mtu}) from externally coupled device into internal muscle fascicle length (L_{ce}) for force computation [23], [33]. The active stiffness arising from length-tension relation along with passive elastic components in the model contributed to total muscle stiffness or compliance.

Three tests were performed to verify control capacity of the virtual prosthetic hand. First, the fingertip forces in flexion and extension were evaluated and found to vary linearly with α command (Fig. 1(d)). It revealed that the α commands of flexor and extensor could produce a well-behaved fingertip force in a given finger configuration. Second, force variability of the biorealistic control system was assessed. The index finger was controlled to press a wooden block by co-activated α commands embedded with signal-dependent noise (SDN) [34], as shown in the first panel of Fig. 1(e). The variability of fingertip force increased with the mean force in proportion. This indicated that the virtual prosthetic hand had the capability of fine force control at low levels of muscle activation.

In the third test, the index finger was driven to press a spring plate with 30 N/m stiffness with a ramp α command to each muscle. Results in Fig. 1(f) showed three phases of control: (1) fingertip position (prior to t_1), (2) combination of position and force (between t_1 and t_2), and (3) force (after t_2). It clearly illustrated that the biorealistic controller could stably handle switch from position control to force control, or both without having to explicitly identify the states. This revealed an important human-like compliant property of biorealistic control. This nature could allow intuitive control of fingertip position and force amid changes in external load during grasping an object.

B. CONTROL OF FINGERTIP COMPLIANCE

Endpoint perturbation test was used to evaluate compliant property of the tendon-driven virtual prosthetic hand. When the index finger was stabilized at an equilibrium position (EP) by activating a pair of constant α motor commands, a

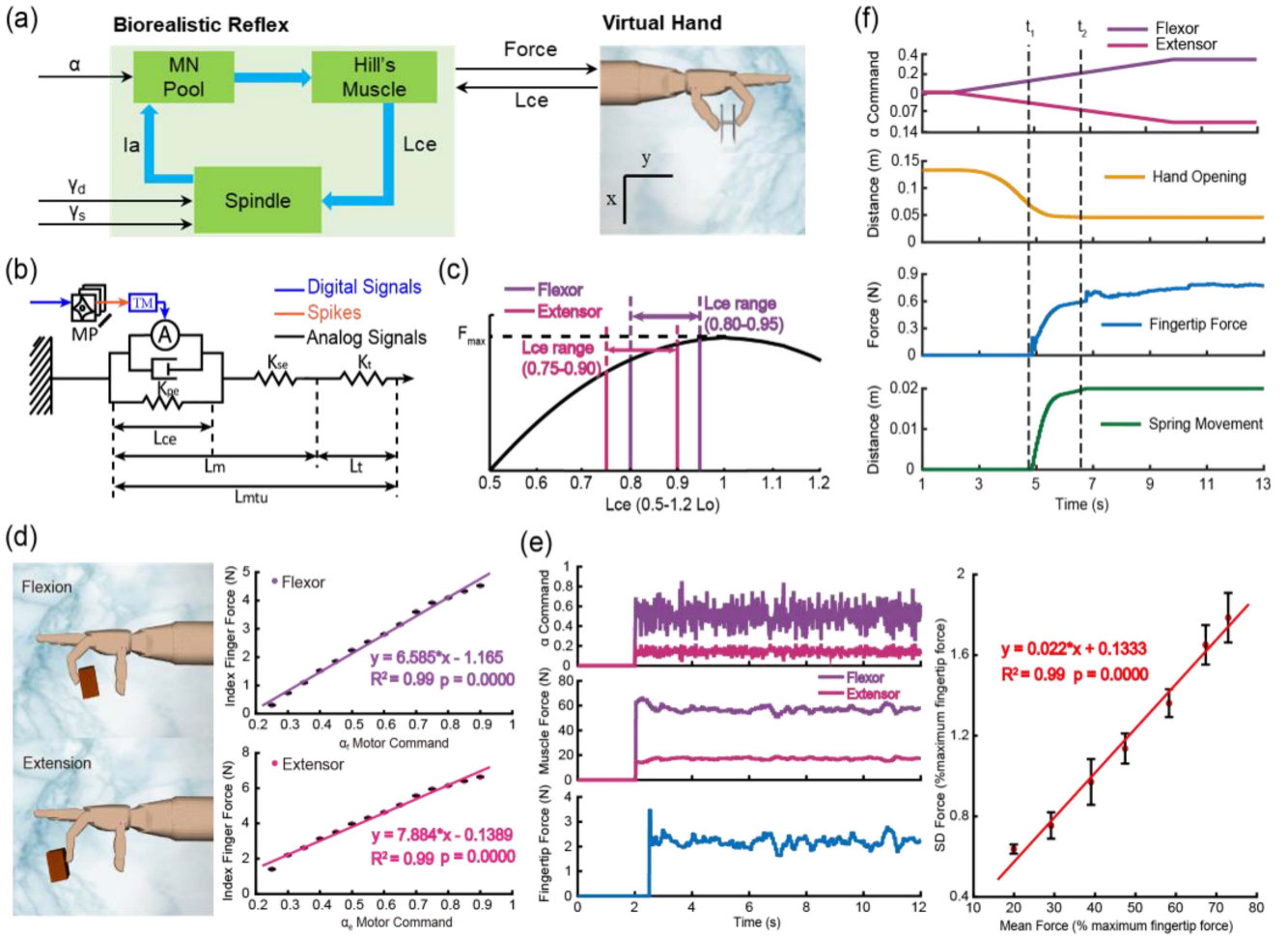

FIGURE 1. **(a) The virtual hand is driven by a pair of biorealistic reflex models. Inputs of the models are α motor commands, γ_s and γ_d commands. (b) A Hill-type muscle model. The active component is activated by a motoneuron pool (MP) via a twitch model (TM). K_{pe}, K_{se} and K_t represent the stiffness of parallel elastic element, series elastic element and tendon. L_{mtu}, L_t, L_m and L_{ce} represent the musculotendinous unit length, tendon length, muscle length and muscle fascicle length. (c) The relationship between measured muscle force and normalized fascicle length in our model. The normalized range of flexor L_{ce} is 0.80 $\sim$ 0.95 L_o, while the range of extensor L_{ce} is 0.75 $\sim$ 0.90 L_o. (d) Force generation in flexion and extension. It shows the experimental scenario and the force responses to α command. (e) Force variability test. It shows the change of α command, muscle force, fingertip force when the signal-dependent noise added and the relationship between SD force and mean force. (f) System responses under α ramp commands to flexor and extensor that control the index finger to press a spring plate of 30 N/m. t_1 is the time of finger contact with the spring plate and t_2 is the time that the spring plate was pressed to its limit position.**

vector of perturbation force was applied to the fingertip, and system's response was shown in Fig. 2(a). The endpoint of finger deviated from the initial EP, then reached to a new EP. The musculotendinous length (L_{mtu}) and fascicle length (L_{ce}) of flexor were shortened and the flexor force was reduced, while the L_{mtu} and L_{ce} of extensor were lengthened and the extensor force was increased according to the length-tension curve (Fig. 1(c)).

Endpoint stiffness ellipses of the index finger and muscle stiffness of flexor and extensor were calculated in Fig. 2(b) and Fig. 2(c). At each EP, the area of endpoint stiffness ellipse increased with the increasing level of antagonistic co-contraction (AC) (Fig. 2(b)). The shape and orientation of endpoint stiffness ellipses were qualitatively similar to those in human multi-joint arm postures [35], [36]. Long axis of the ellipse represented the maximum stiffness direction, and short axis signified the minimum stiffness direction, which corresponded to the direction of finger movement.

Muscle stiffness represented the relation between changes in muscle force and fascicle length. Muscle stiffness was proportional to α motor command (Fig. 2(c)), as well as muscle force produced as in Fig. 2(d). These properties were similar to those observed in physiological measurements in mammalian animals and humans [28], [37]. These findings confirmed that the virtual hand encompassed the similar compliant property of human neuromuscular system.

C. REFLEX CONTRIBUTION TO MUSCLE AND ENDPOINT STIFFNESS

In the biorealistic reflex model, Ia afferent from spindle model regulated the activation of motoneuron pools, closing the loop

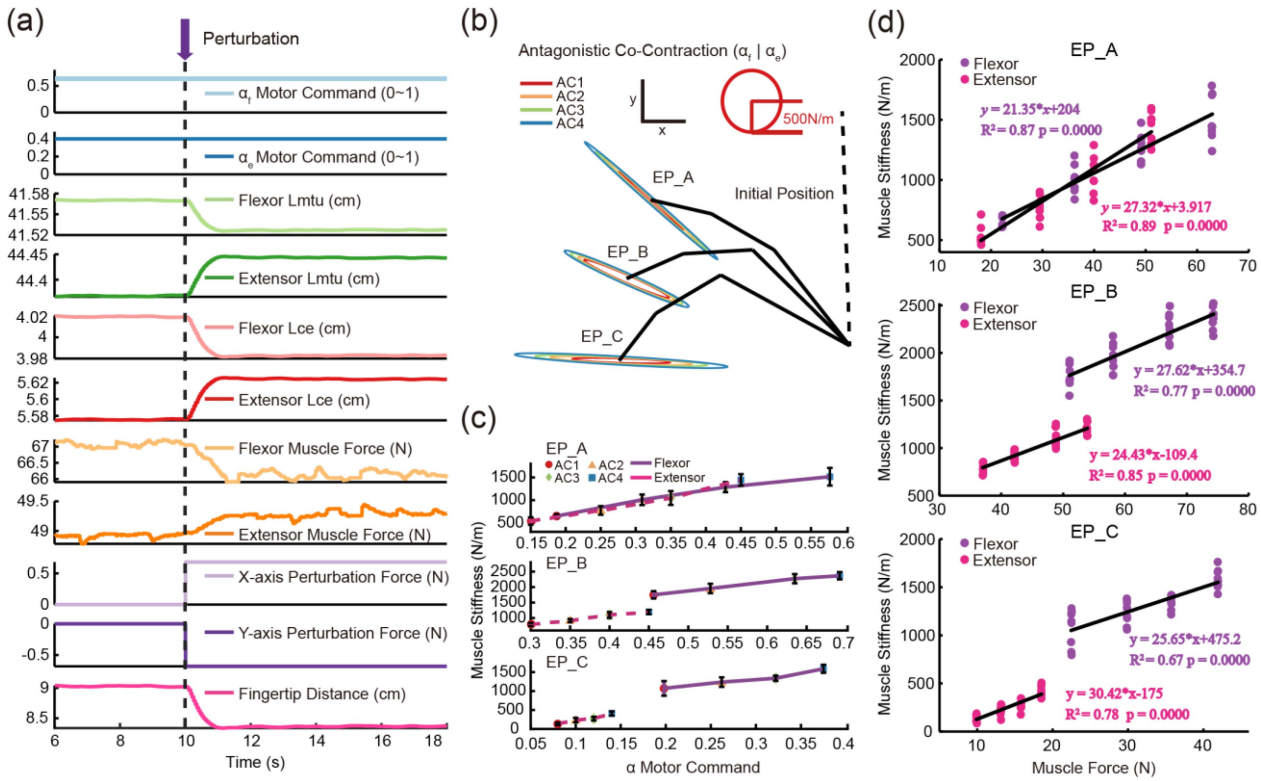

FIGURE 2. **Results of closed-loop perturbation experiments at equilibrium positions. (a) An example of profiles of variables in the closed-loop perturbation experiment. (b) Stiffness ellipses of endpoint with four increasing levels of muscle antagonistic co-contraction (AC) at equilibrium position (EP) EP_A, EP_B and EP_C on the x-y horizontal plane. Four ellipses are superimposed at each EP, and each level of AC is identified by a different color. The calibration of the ellipse is provided by a standard circle on the top right corner, which represents an isotropic stiffness of 500 N/m. (c) Muscle stiffness of flexor and extensor at EP_A, EP_B and EP_C under four increasing AC levels. (d) Muscle stiffness in response to muscle force at EP_A, EP_B and EP_C.**

of reflex. Here we evaluated to what extent Ia afferent may affect muscle stiffness and endpoint compliance.

Endpoint stiffness ellipses in open-loop and closed-loop at the same levels of AC were illustrated in Fig. 3. Compared to stiffness ellipses in closed-loop, the area of stiffness ellipses in open-loop appeared smaller with no change in shape and orientation at each EP. Thus, Ia afferent altered mainly the magnitude of stiffness ellipses.

Specifically, the contribution of reflex pathway was assessed with a set of perturbation tests under four different levels of AC at EP_B. Changes in eigenvalues and area of ellipses of endpoint stiffness matrix, as well as the change in muscle stiffness were calculated using eq. (3). Results were summarized in Fig. 3(b-d). Compared to open-loop model, changes in closed-loop model were manifested mainly as an increase in the major axis of endpoint stiffness ellipses at 10.84 ± 3.94 % and the minor axis at 11.34 ± 3.13 % (Fig. 3(b)), increase in the total area of endpoint stiffness ellipse at 23.50 ± 7.80 % (Fig. 3(b)), and increase in muscle stiffness at 16.16 ± 12.33 % for flexor and 8.79 ± 9.54 % for extensor (Fig. 3(d)). But there was little or no influence on the shape and orientation of endpoint stiffness ellipses (Fig. 3(c)). This may be due to the fact that joint configurations dominated the influence to shape and orientation of endpoint stiffness. These showed that Ia afferent in neuromorphic reflex model did enhance fingertip and muscle stiffness to a certain extent consistent with experimental findings [38], [39], [40].

D. ADAPTIVE REGULATION OF COMPLIANCE IN GRASPING A SOFT SPRING

Compliant operation of the virtual hand interacting with a soft object (spring) was further evaluated. At steady state of grasping a spring in Fig. 4(b), a perturbation force was applied to the tendon of flexor or extensor, respectively, and the stiffness of fingertip and muscle was calculated. Fig. 4(a) depicted a representative trial of variables of the finger moving from the original EP to a new EP with a perturbation force (17 N) applied to flexor tendon. The L_{mtu} and L_{ce} of flexor were shortened and flexor force was reduced; while the L_{mtu} and L_{ce} of extensor were lengthened and extensor force was increased. The index fingertip force was greater due to added perturbation force, pressing the spring further in.

It was observed that fingertip stiffness matched to the spring stiffness at the finger-spring contact as in Fig. 4(c) (R^2=1, p = 0.0000). This was consistent with the mechanical constraint of impedance matching between objects at the interacting interface in the vertical direction [41] based on the physical law of action and reaction in opposing forces. Muscle stiffness varied linearly with muscle activation levels, and external spring stiffness as shown in Fig. 4(d).

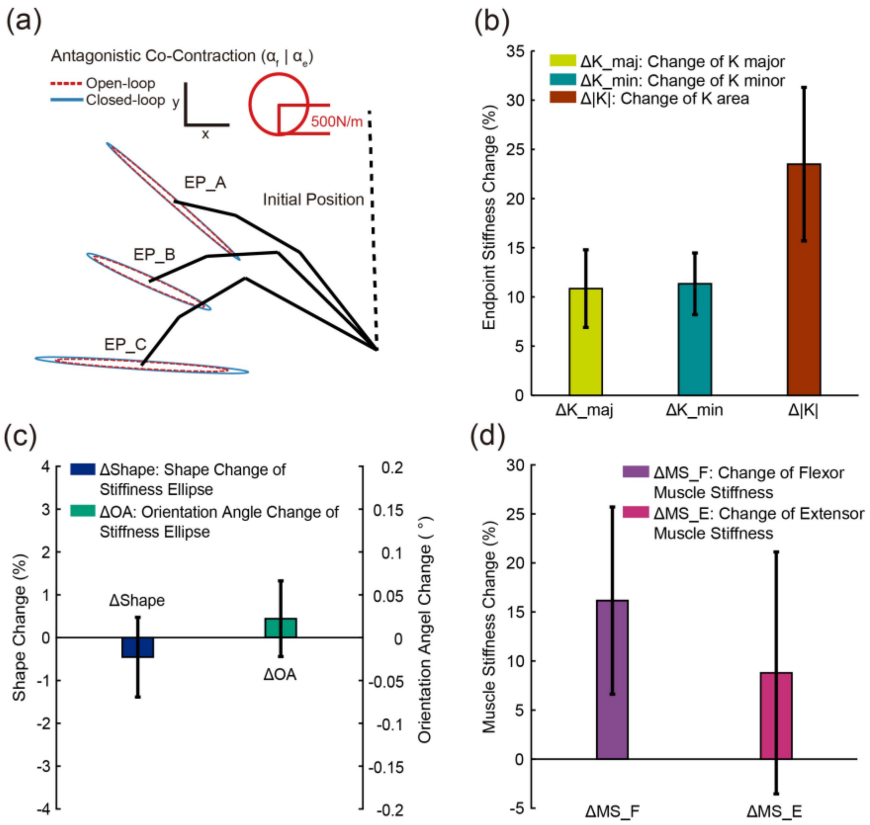

FIGURE 3. Contribution of stretch reflex on endpoint and muscle stiffness. (a) Presents stiffness ellipses of endpoint at three EPs in open-loop and closed-loop perturbation experiments. Red dashed line represents open-loop stiffness ellipses and blue solid line represents those in closed-loop. (b-c) Effects on stiffness ellipse change of reflex feedback at EP_B. The magnitude, shape and orientation of endpoint stiffness are shown in (b) and (c). (d) Depicts the change of muscle stiffness of flexor and extensor caused by the reflex contribution.

Spring stiffness determined the degree of spring deformation, which affected muscle length L_{ce}, hence, muscle force/stiffness at equilibrium with a given muscle activation. Fig. 4(d) illustrated an adaptive adjustment of muscle force and stiffness with changes in L_{ce} from length-tension curve and reflex compensation for a given background activation of flexor and extensor. The range of stiffness adjustment was represented by the variability, or standard deviation (SD), in muscle stiffness (Fig. 4(e)). It was noted that the flexor SD appeared to have an upward trend ($R^2 = 0.90$, $p = 0.0523$), while the trend in extensor was not apparent ($R^2 = 0.07$, $p = 0.7434$) due to little change of α command, implying that background activation may also affect the range of stiffness adjustment. This was corroborated with the fact that the length-tension curve in the model was a quadratic curve scaled with activation level.

III. DISCUSSION

Human hand control presents a perfect model for prosthetic control. Humans achieve dexterous grasp through compliant actuation of muscles and rich sensory afferents from proprioceptors and cutaneous receptors [18]. The compliant control can adjust hand stiffness when grasping brittle or soft objects without violating them. The viscoelasticity of skeletal muscle arises from length-tension and force-velocity properties of muscular fiber [28], [29], [42], [43], and the dynamic property of muscle results from activation and contraction dynamics of muscle fibers [30], [43]. The monosynaptic stretch reflex compensates muscle length changes and regulates to a certain degree the compliance of neuromuscular system [40], [44], [45], [46]. A large body of empirical data are available for comparison of biorealistic controller properties [30], [35], [38], [41], [47], [48], [49], [50].

In this study, a virtual twin of a biorealistic prosthetic hand is developed with computational models of neuromuscular reflex control. The prosthetic controller incorporated a Hill's muscle model [51], a spindle model [19], spiking motoneuron models [52], and a monosynaptic stretch reflex model [32] in neuromorphic hardware chips [53]. Contact sensors embedded at fingertips of the hand allow tactile information to be delivered to amputees through a non-invasive neural interface using evoked tactile sensations (ETS) [27]. The purpose here is to reveal that the virtual prosthetic hand exhibits qualitatively similar behaviors to human neuromuscular reflex system. To our knowledge, this is the first computational model that can capture human-like compliant properties emerging from biologically realistic models.

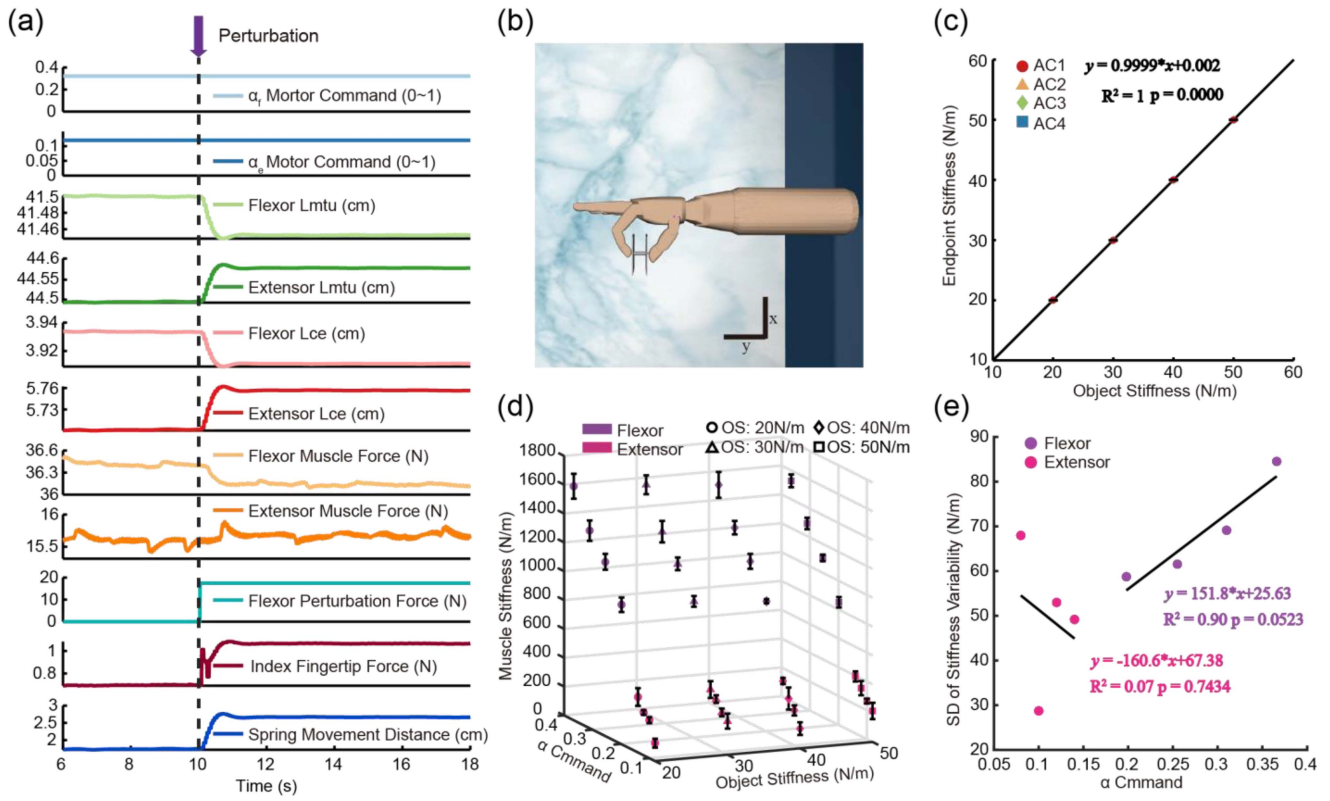

FIGURE 4. **Results of perturbation experiments in grasping spring plates of different stiffness. (a) An example of profiles of variables in perturbation experiments when grasping a spring plate. (b) The experimental scenario that the index finger presses a soft spring plate. The coordinate system indicates the direction of the horizontal plane. (c) Depicts endpoint stiffness when grasping objects of different stiffness under four levels of AC. Linear correlation between endpoint stiffness and object stiffness is y=0.9999*x+0.002 (R^2=1, p=0.0000). (d) 3-D curve in muscle stiffness of flexor and extensor under different AC levels when grasping various compliant spring plates. (e) The standard deviation (SD) of muscle stiffness in grasping springs of various stiffness at different α commands.**

Switching force and position control according to external load is a natural ability of human motor control [54]. Results in Fig. 1 verify that the biorealistic hand prosthesis captures this nature of human compliant control. The fingertip force in flexion and extensor can be well controlled by the α commands (or surface EMGs) through the muscle model with modulation of muscle fascicle length and reflex (Fig. 1(d)). Fingertip force variability with signal-dependent noise (SDN) in the input illustrates a linear scaling with respect to the mean force (Fig. 1(e)). This property allows for more delicate grasp tasks of brittle objects that requires precise and low levels of fingertip force and stiffness. Since muscle (or fingertip) stiffness was proportional to muscle (or fingertip) force (Fig. 2(d), 4(d)), the ability to regulate stiffness in the muscle or by co-contracting antagonistic muscles is crucial for dexterous functions of the prosthetic hand. For example, in grasping a soft spring plate as shown in Fig. 1(f), the finger underwent switching in three phases of control according to external load conditions, i.e., initial position control before contact, both position and force control after contact, and then force control with the spring fully pressed. This ability to naturally switch its control mode according to external loads is similar to that of human [54]. The natural compliant control is advantageous over conventional prosthetic/robotic hands that require sensors to detect external loading conditions in order to switch control modes [41], [54], [55].

Fingertip stiffness regulation by co-contracting antagonistic muscles is mainly manifested in magnitude, while joint configuration plays a significant factor for the shape and orientation of endpoint stiffness ellipse as illustrated in Fig. 2. These results were qualitatively similar to those in observed humans in magnitude, shape and orientation [22], [35], [50], [56]. Specially, muscle force and stiffness were proportionally to each other and with α motor commands (Fig. 2(d), Fig. 4(d)) as observed in animal and human studies [28], [37], [38], [57]. It is noted that the value of muscle stiffness calculated in the model was smaller than that measured in humans [58]. This discrepancy is due to the fact that the maximum muscle force set in the model (at 100 N [24]) was an order of magnitude smaller than actual maximal force in human muscle [58]. It is also observed that in free-moving conditions, fingertip positions could be maintained by co-varying activations of a pair of antagonistic muscles (Fig. 2(b)). This suggests that equilibrium position could emerge as a result of length-dependent forces generated by agonist-antagonist muscles [59].

Spindle model used here was constructed using data collected from animal studies [19], and was verified to generate reflex behaviors as those of human spindle [22], [60], [61], as well as those from microneurography [62], [63]. The contribution of monosynaptic reflex to enhance muscle stiffness in the model was estimated at 16.16 ± 12.33 % and 8.79 ± 9.54 % for flexor and extensor, respectively (Fig. 3(d)), which was close to the range of measured values at 18-44 % of total stiffness in the first dorsal interosseous muscle in humans [38]. The lower contribution may be due to the fact that reflex gain in our model was moderate (about 10%) to avoid instability [23]. The three parameters of endpoint stiffness ellipses (area, major and minor axes) could not be modulated independently by reflex, since it changed α commands of flexor and extensor. This was evident with results in Figs. 2 and 3. Therefore, α commands determined magnitudes of stiffness ellipse (Fig. 2(b)), while joint configuration affected mainly orientation and shape of the stiffness ellipse (Fig. 3(c)). These properties are a necessary consequence of mechanics in the model.

A striking new revelation comes from investigation of interaction of the virtual hand with a spring object as demonstrated in Fig. 4. At steady state of grasp, the finger stiffness at contact point matched to the spring stiffness at the finger-spring interface as in Fig. 4(c), consistent with the requirement at mechanically interacting interface [41]. The process of matching fingertip stiffness is adaptively regulated by the muscle model (also see a video demonstration in Supplementary Materials).

For a given spring stiffness, a constant α command may be issued to the flexor muscle with a strength not calculated exactly to produce a matching fingertip stiffness. But the matching is achieved with adaptive adjustment of muscle stiffness endowed by the muscle model. If the fingertip stiffness initially produced is greater than the spring stiffness, the spring will be pressed in further, and the L_{ce} of flexor muscle will be shortened. According to the length-tension curve, the force and stiffness of the muscle/fingertip will be reduced. This adjustment process will continue until the force and stiffness at the fingertip equal to those of the spring. An opposite process in the extensor muscle takes place to aid the adjustment of fingertip force and stiffness. On the other hand, if the initial fingertip stiffness is smaller than the spring stiffness, the length-tension curve of flexor and extensor will make concerted adjustments to increase fingertip force and stiffness until a balance at fingertip-spring is reached. This automatic adjustment mechanism depicts the process of "adaptive stiffness regulation" (see video demonstration in the Supplementary Materials). With this mechanism, one does not have to calculate an exact α command to flexor and extensor when grasping a soft object. An estimate of rough α command may be issued, and the adaptive mechanism will allow fine tuning of muscle force and stiffness to match those of the spring. This is one of the advantages of compliant control in humans.

A secondary mechanism via reflex will also participate in the adaptive stiffness regulation process through Ia afferent induced by L_{ce} changes. However, its effect may be limited due to low reflex gain [23] and a delay (about 200 ms [61]) in afferent signal transmission. Nevertheless, the two adaptive mechanisms work in concert to fine tune muscle or fingertip stiffness to match the spring stiffness. The range of stiffness modulation by the length-tension curve and reflex under a given background activation showed an increasing range with the AC level (Fig. 4(e)). This is consistent with fact that the length-tension curve in the muscle model is scaled with α command. This property of adaptive stiffness regulation will be beneficial for the biorealistic prosthetic hand to handle soft objects.

We showed here that the comprehensive model exhibits compliant properties qualitatively similar to those obtained in human or animal physiological experiments. The emerging behaviors originate from the physiologically realistic submodels, i.e., neurons, muscles and spindle, which constitute the biorealistic neuromorphic reflex control. Second, the muscle model was coupled to the prosthetic hand with anatomically realistic parameters. This ensures the physiological plausibility for amputees to operate the prosthetic hand. This in turn substantiated our previous findings of improved performance in human experiments [25]. It is interesting to note that this modeling approach can be further combined with a surgical procedure that creates a better agonist-antagonistic residual muscle pair for prosthetic control [64]. Also replacing our model of intact muscle with one of residual muscle [65] would still preserve the compliant properties of the prosthetic hand.

There are limitations, however, in this study. First, we simplified simultaneous control of multiple degrees of freedom in prosthetic fingers [1], [66] to a single tendon force control, and reduced decoding multi-channel EMG signals for commands [4], [66] to intuitive control by flexor and extensor sEMGs. Second, the neuromorphic model is still preliminary compared to biological neuromuscular reflex system. The neural transmission delay of the spindle was about 200 ms [61], and the overall computational delay between α command input to force output was about 400 ms. Ib reflex of the Golgi tendon organ (GTO) was omitted in this model for its low gain in physiological condition [22], [67], despite significant roles in lower limb weight bearing [68]. Nevertheless, human-like neuromuscular reflex control was demonstrated necessary and sufficient to provide a good neural compatibility with the sensorimotor system and superior task performance by amputees using the biorealistic prosthetic hand [24], [25].

There are several implications for future research. (1) This study along with our previous work [24], [25] leads to a novel direction for developing a new generation of prosthetic hand with human-like properties i.e., a comprehensive replica of human neuromuscular control that can adjust stiffness over a wide range of operating conditions [69]; (2) the biorealistic hand can be seamlessly neural compatible with the human sensorimotor system, thus, facilitate amputees for more dexterous control using an antagonistic muscle pair as command sources [64]; (3) the virtual hand developed here may establish a useful training platform for amputees to familiarize

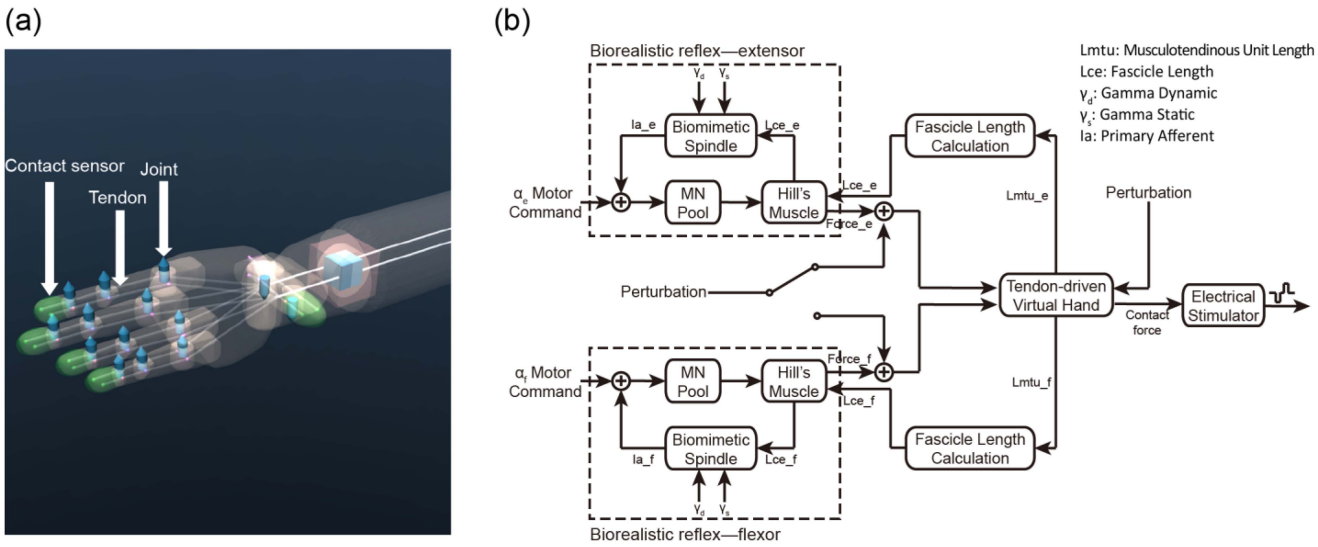

FIGURE 5. **(a) Virtual hand in MuJoCo. The virtual hand has five contact sensors, fourteen joints, ten tendons and ten actuators. (b) The block diagram of the integrated virtual hand system. It consists of a tendon-driven virtual hand, a pair of neuromorphic muscles and a sensory feedback system. Force perturbations can be applied at fingertip, or the tendon of flexor/extensor in the perturbation experiments.**

control of biorealistic prosthetic hands; and (4) the computational modeling approach can promote reverse engineering to understand neural mechanisms of brain control for hand movements in humans.

IV. CONCLUSION

In this study, a virtual hand with a pair of neuromorphic muscles and a sensory feedback system was integrated in MuJoCo environment. The model incorporated biorealistic elements of human neuromuscular reflex. A comprehensive evaluation showed that the virtual twin of the biorealistic prosthetic hand could maintain a stable hand opening for grasp, adjust control mode according to the external loading condition, and adaptively regulate hand stiffness to match that of grasped object. This study confirms that the virtual hand is capable of recapturing human-like neuromuscular properties of compliance, adaptative stiffness regulation, and fine control of fingertip force. These findings lead to new insights into how human-like neuromuscular reflex may facilitate prosthetic control of the virtual hand and suggest a teleological correlation between human-like neuromuscular control and neural compatibility in hand prosthesis.

V. MATERIALS AND METHODS

A. VIRTUAL PROSTHETIC HAND DEFINITION

MuJoCo is a virtual environment using a physics engine that has fast and accurate computational power to calculate contact interactions between objects. It runs the simulation at a frequency of 500 Hz. We developed a tendon-driven virtual prosthetic hand (Fig. 5(a)) in the MuJoCo (Version 2.0) environment of real-time computation. Tendon-driven structure was added on the virtual prosthetic hand based on the provided vMPL hand (Johns Hopkins Applied Physics Lab, Laurel, MD) to fit the neuromorphic control (Fig. 5(a)). The added ten tendons started from the forearm and passed through fixed anchor points to the tip of each finger according to the anatomy of hand musculature [70]. On the palmar and dorsal side of each joint, an anchor point was set on the joint, which rotated with joint movement. The rotation axis of each joint was parallel to the palmar side of the hand to make the joint flex or extend. All anchor points on the palmar side were coupled by the flexor tendon, while those on the dorsal side were coupled by the extensor tendon. The tendon compliance was considered in the muscle model with a serial tendon stiffness K_t (Fig. 1(b)), and the stiffness parameter of the elastic components was shown in Table S1. The value of K_t was much greater that of K_{se}, and K_t still contributed to the overall stiffness at the fingertip. Tendons were actuated by ten muscles (actuators). Here the maximum force of each muscle generated was set to 100 N.

Overall, the modified virtual hand as in Fig. 5(a) has 5 contact sensors: one on the distal phalangeal segment of each finger; 14 joints: two joints in the thumb and three joints in other fingers; 10 tendons: two for each finger; and 10 actuators: five pulling flexion tendons and five pulling extension tendons. Each tendon wrapped around all joints of the digit.

B. INTEGRATION OF VIRTUAL PROSTHETIC HAND SYSTEM

The virtual prosthetic hand system was integrated with a pair of biorealistic controllers and a sensory feedback system. The biorealistic reflex models replaced the original agonist-antagonist muscle pair in situ to compute muscle forces to actuate virtual tendons to produce movements in the MuJoCo environment. The physiological plausibility of this model was achieved by physiologically realistic properties included and anatomically realistic parameters specified according to the

anatomy of target muscles *in situ*. Contact sensors at fingertips delivered force information to amputees using a sensory feedback system when interacting with objects (Fig. 5(b)).

The biorealistic controller emulated a monosynaptic stretch reflex loop by modeling essential elements in the neuromuscular system, which was implemented on a programmable Very-Large-Scale-Integration (VLSI) in real-time using FPGA chips (Xilinx Spartan-6) [23]. It consisted of models of motoneuron pool including 768 spiking neurons [52], one Hill-type muscle model [51], one spindle model with 128 randomly unsynchronized outputs [19] and monosynaptic stretch reflex [32]. The input of the biorealistic controller was α motor command (or sEMG signal from a residual muscle), which activated motoneuron pool following Henneman's size-principle [71]. The activated spiking signal was converted to a twitch signal via a low-pass filter twitch model to drive the Hill's muscle model. Muscle forces from neuromorphic muscle models of flexor and extensor pulled the corresponding tendon individually to control the movement of the prosthetic finger. The spindle model accepted inputs of fascicle length, gamma static (γ_s) and gamma dynamic (γ_d) commands to send a volley of Ia afferents back to motoneuron pool to close the reflex loop. The neuromorphic hardware chips were linked to the virtual environment and transferred data bidirectionally by a universal serial bus (USB) interface.

The sensory feedback system received contact force information at fingertips in MuJoCo by user datagram protocol (UDP) network communication and transferred it to electrical pulses to amputees via a non-invasive neural interface exploiting ETS in amputees with transcutaneous electrical nerve stimulation (TENS) [27], [72].

C. ESTIMATION OF FASCICLE LENGTH OF MUSCLE

Fascicle length (L_{ce}) plays a vital role in the biorealistic reflex model. It can modulate the proprioception afferents from spindle model and exert muscle force depend on length-tension property in Hill-type muscle model. However, the exact value of L_{ce} at different finger configurations is unclear from the literature. We need to estimate it according to the available realistic parameters of target muscles in situ.

In our virtual prosthetic system, the anatomically length information was derived from a pair of antagonistic muscles: flexor digitorum profundus (FDP) and extensor digitorum (ED), which is commonly used to control prosthetic hand by forearm amputees. The real physiological length information of these two muscles was listed in bold in Table S1 [73]. Due to the lack of real musculoskeletal structure in the virtual environment, we set the initial virtual tendon length of flexor and extensor as the real musculotendinous unit length (L_{mtu}) on the resting position. During the movement of the hand grasp, the change of the virtual tendon length was equivalent to the change of L_{mtu} (ΔL_{mtu}). In the Hill's muscle model of biorealistic reflex (Fig. 1(b)), the change of fascicle length (ΔL_{ce}) could be estimated by ΔL_{mtu} based on Luo's calculation algorithm [23], [33].

In the integrated virtual hand, the calculated maximum ΔL_{mtu} of flexor and extensor was 1.11 and 1.52 cm, and the corresponding ΔL_{ce} of flexor and extensor was 0.72 and 0.99 cm. We selected the normalized range of L_{ce} of flexor and extensor was $0.80 \sim 0.95\ L_o$ (optimal length to peak force) and $0.75 \sim 0.90\ L_o$ respectively (Fig. 1(c)). Hence the actual L_o in flexor and extensor on the initial position we set was 4.8 and 6.6 cm, as shown in Table S1. The selected operating range is in the ascending limb of length-tension curve due to the reason of stability.

D. CONTROL CAPACITY EVALUATION

We designed three sets of tests to evaluate the control capacity of the virtual prosthetic hand. The first test was to evaluate the capacity of force generation in flexion and extension. The index finger was stabilized at a fixed configuration by an activation pair of flexor and extensor (α_f=0.20 and α_e=0.14). Two wooden blocks were placed at the vertical direction of 0.5 cm from the fingertip and the dorsal fingertip (left panel in Fig. 1(d)). Continuously increasing the α_f command or α_e command individually to make the fingertip or dorsal fingertip press the wooden block to generate the touching force, and the flexion and extension force were shown in Fig. 1(d).

The second test was to evaluate the effect of intrinsic motor noise of control signals on fingertip force variability. Fingertip force variability was characterized by the standard deviation (SD) of the fingertip contact force. A source of neuromuscular signal-dependent noise (SDN) was introduced to the motor commands of each muscle. The SDN was a Gaussian distributed noise with a standard deviation (SD) proportional to the magnitude of the motor command (α) with a constant coefficient of variation ($CV = SD/\alpha = 0.2$) [22], [34]. A pair of antagonistic α commands with SDN noise was activated to control the virtual hand to press the right wooden block. Each experiment lasted 12 seconds and the last 2 seconds of the fingertip force were calculated for the subsequent analysis. Each pair of α commands was repeated 5 times at each of seven different target force levels ranging from approximately 20 to 80 % maximum fingertip force.

The third test is to investigate the different control phases when interaction with different external environments. An eight-second ramp input with α commands was co-activated to drive the index finger pressing a spring plate as in Fig. 1(a). The stiffness of the spring plate was 30 N/m and the maximum contraction distance of the spring was 2 cm.

E. EVALUATION OF COMPLIANT PROPERTIES AT EQUILIBRIUM POSITIONS

To measure the endpoint stiffness of fingertip and muscle stiffness, a small vector of perturbation force was applied on the tip of index finger when the finger stabilized at the equilibrium position (EP), which enforced the finger deviated to the new EP. For each EP, four different pairs of α commands of antagonistic muscles drive the index finger to the stable position.

Eight various orientations of perturbation force were added to calculate the matrix of endpoint stiffness, the deviation of the fingertip moving distance was about 0.5 cm. Endpoint stiffness matrix $\boldsymbol{K}$ at fingertip was estimated using the least square method:

$$\begin{bmatrix} Fx \\ Fy \end{bmatrix} = \begin{bmatrix} Kxx & Kxy \\ Kyx & Kyy \end{bmatrix} \begin{bmatrix} dx \\ dy \end{bmatrix} \quad (1)$$

For the stiffness matrix $\boldsymbol{K}$ of the endpoint, it could be expressed by a stiffness ellipse:

$$\begin{bmatrix} Fx \\ Fy \end{bmatrix} = \boldsymbol{K} \begin{bmatrix} \cos t \\ \sin t \end{bmatrix} \quad (2)$$

In (1) and (2), the four coefficients Kxx, Kxy, Kyx and Kyy are the four elements of the stiffness matrix $\boldsymbol{K}$. Fx and Fy represent the reaction forces in x and y directions, dx and dy are the unit distances in the x and y coordinate axis.

Muscle stiffness was defined as the derivative of the change in muscle force with respect to the change in muscle fascicle length.

F. QUANTIFICATION OF REFLEX CONTRIBUTION

Reflex pathway delivers Ia afferent to the spinal cord to regulate the movement of the limb and also enhances muscle stiffness [39]. Ia afferent pathway was artificially cut off to eliminate the role of reflex in biorealistic controller and the contribution of reflex was evaluated in enhancing muscle and endpoint stiffness. Lack of reflex feedback, a pair of biorealistic controllers was in an open-loop state, and the same paradigm of the perturbation experiments as in closed-loop was applied on the index finger to calculate endpoint stiffness ellipse and muscle stiffness at different configurations under four increasing antagonistic co-contraction (AC) levels.

The change of endpoint stiffness ellipse and muscle stiffness was quantified using the following equation:

$$Change\ in\ Stiffness = \frac{Stiffness_{closed\_loop} - Stiffness_{open\_loop}}{Stiffness_{open\_loop}} * 100\% \quad (3)$$

G. COMPLIANT GRASPING OF A SOFT SPRING

A simulation experiment was used to explore how the compliant properties of biorealistic reflex were functioning when grasping soft objects. A set of spring plates of different stiffness was fixed at the same position in MuJoCo (Fig. 4(b)). Four pairs of α motor commands that stabilized the index finger at EP_C in closed-loop perturbation experiments were used as driving signals to control the index finger grasping a spring plate of different stiffness. The spring plate kept contracting until the finger force was equal to the spring resistance force, in which the finger-spring combination was maintained at a steady state. A perturbation force was added on the flexor or extensor tendon to change the fingertip pressing force to move the spring plate until a balance again appeared at the finger-spring interface. For each experimental session, a perturbation force was added on the flexor tendon and extensor tendon three times respectively and it was adjusted as the increasing background activation of flexor and extensor to move the spring plate about 1 cm.

Muscle stiffness varied with the external object stiffness under the same background activation. The range of muscle stiffness was characterized as the standard deviation (SD) of muscle stiffness produced by grasping objects of different stiffness and the relation between SD of muscle stiffness variability and α command was shown in Fig. 4(e).

SUPPLEMENTARY MATERIALS

Table S1. Parameters of the muscle model at the resting position. Video S1. Virtual hand interaction with a spring showing adaptive stiffness regulation.

ACKNOWLEDGMENT

Authors appreciate lab engineer, Mr. R. Yue, who set up the neuromorphic computing hardware for this study.

REFERENCES

[1] J. M. Hahne, M. A. Schweisfurth, M. Koppe, and D. Farina, "Simultaneous control of multiple functions of bionic hand prostheses: Performance and robustness in end users," *Sci. Robot.*, vol. 3, no. 19, Jun. 2018, Art. no. eaat3630.

[2] M. Ortiz-Catalan, E. Mastinu, P. Sassu, O. Aszmann, and R. Brnemark, "Self-contained neuromusculoskeletal arm prostheses," *New England J. Med.*, vol. 382, no. 18, pp. 1732–1738, Apr. 2020.

[3] M. D. Paskett et al., "Activities of daily living with bionic arm improved by combination training and latching filter in prosthesis control comparison," *J. NeuroEng. Rehabil.*, vol. 18, no. 1, Feb. 2021, Art. no. 45.

[4] L. Schmalfuss et al., "A hybrid auricular control system: Direct, simultaneous, and proportional myoelectric control of two degrees of freedom in prosthetic hands," *J. NeuroEng.*, vol. 15, no. 5, Oct. 2018, Art. no. 056028.

[5] C. Cipriani et al., "Online myoelectric control of a dexterous hand prosthesis by transradial amputees," *IEEE Trans. Neural Syst. Rehabil. Eng.*, vol. 19, no. 3, pp. 260–270, Jun. 2011.

[6] S. B. Godfrey et al., "Softhand at the cybathlon: A user's experience," *J. NeuroEng. Rehabil.*, vol. 14, no. 1, Nov. 2017, Art. no. 124.

[7] K. Østlie, I. M. Lesjø, R. J. Franklin, B. Garfelt, O. H. Skjeldal, and P. Magnus, "Prosthesis rejection in acquired major upper-limb amputees: A population-based survey," *Disabil. Rehabil.: Assistive Technol.*, vol. 7, no. 4, pp. 294–303, Jul. 2012.

[8] L. Jones and S. Lederman, *Human Hand Function*, Eds., New York, NY, USA: Oxford Univ. Press, 2006.

[9] J. R. Napier, "The prehensile movements of the human hand.," *Bone Joint J.*, vol. 38-B, no. 4, pp. 902–913, Jan. 1956.

[10] C. L. Taylor and R. J. Schwarz, "The anatomy and mechanics of the human hand," *Artif. Limbs*, vol. 2, no. 2, pp. 22–35, May 1955.

[11] E. A. Biddiss and T. T. Chau, "Upper limb prosthesis use and abandonment: A survey of the last 25 years," *Prosthetics Orthotics Int.*, vol. 31, no. 3, pp. 236–257, Jan. 2007.

[12] B. Stephens-Fripp, G. Alici, and R. Mutlu, "A review of non-invasive sensory feedback methods for transradial prosthetic hands," *IEEE Access*, vol. 6, pp. 6878–6899, Jan. 2018.

[13] R. Deimel and O. Brock, "A novel type of compliant and underactuated robotic hand for dexterous grasping," *Int. J. Robot. Res.*, vol. 35, no. 1–3, pp. 161–185, Jan. 2016.

[14] C. Piazza, G. Grioli, M. G. Catalano, and A. Bicchi, "A century of robotic hands," *Annu. Rev. Control, Robot., Auton. Syst.*, vol. 2, no. 1, pp. 1–32, May 2019.

[15] A. Verl, A. Albu-Schäffer, O. Brock, and A. Raatz, *Soft Robotics: Transferring theory to Application*, Eds., Berlin Germany: Springer, 2015, Art. no. 291.

[16] D. R. Higueras-Ruiz, K. Nishikawa, H. Feigenbaum, and M. Shafer, "What is an artificial muscle? A comparison of soft actuators to biological muscles," *Bioinspiration Biomimetics*, vol. 17, no. 1, 2021, Art. no. 011001.
[17] M. Manti, V. Cacucciolo, and M. Cianchetti, "Stiffening in soft robotics: A review of the state of the art," *IEEE Robot. Automat. Mag.*, vol. 23, no. 3, pp. 93–106, Sep. 2016.
[18] N. Lan et al., "Next-generation prosthetic hand: From biomimetic to biorealistic," *Research*, vol. 2021, Mar. 2021, Art. no. 4675326.
[19] M. P. Mileusnic, I. E. Brown, N. Lan, and G. E. Loeb, "Mathematical models of proprioceptors. I. control and transduction in the muscle spindle," *J. Neurophysiol.*, vol. 96, no. 4, pp. 1772–1788, Oct. 2006.
[20] D. Song, G. Raphael, N. Lan, and G. E. Loeb, "Computationally efficient models of neuromuscular recruitment and mechanics," *J. Neural Eng.*, vol. 5, no. 2, Jun. 2008, Art. no. 008.
[21] S. Li et al., "Coordinated alpha and gamma control of muscles and spindles in movement and posture," *Front. Comput. Neurosci.*, vol. 9, Oct. 2015, Art. no. 122.
[22] X. He, Y. Du, and N. Lan, "Evaluation of feedforward and feedback contributions to hand stiffness and variability in multijoint arm control," *IEEE Trans. Neural Syst. Rehabil. Eng.*, vol. 21, no. 4, pp. 634–647, Jul. 2013.
[23] C. M. Niu, Q. Luo, C. Chou, J. Liu, M. Hao, and N. Lan, "Neuromorphic model of reflex for realtime human-like compliant control of prosthetic hand," *Ann. Biomed. Eng.*, vol. 49, no. 2, pp. 673–688, Feb. 2021.
[24] Q. Luo, C. M. Niu, J. Liu, C. - H. Chou, M. Hao, and N. Lan, "Evaluation of model-based biomimetic control of prosthetic finger force for grasp," *IEEE Trans. Neural Syst. Rehabil. Eng.*, vol. 29, pp. 1723–1733, 2021.
[25] Q. Luo et al., "Biorealistic control of hand prosthesis augments functional performance of individuals with amputation," *Front. Neurosci.*, vol. 15, Dec. 2021, Art. no. 1668.
[26] Z. - Z. Zhang, J. Zhang, C.-X. M. Niu, M. - Z. Hao, and N. Lan, "An integrated virtual hand platform for evaluation of model-based control of hand prosthesis," in *Proc. IEEE Int. Conf. Real-time Comput. Robot.*, 2021, pp. 287–291.
[27] M. Hao et al., "Restoring finger-specific sensory feedback for transradial amputees via non-invasive evoked tactile sensation," *IEEE Open J. Eng. Med. Biol.*, vol. 1, pp. 98–107, 2020.
[28] G. C. Joyce and P. M. H. Rack, "Isotonic lengthening and shortening movements of cat soleus muscle," *J. Physiol.*, vol. 204, no. 2, pp. 475–491, Oct. 1969.
[29] F. E. Zajac, "Muscle and tendon: Properties, models, scaling, and application to biomechanics and motor control," *Crit. Rev. Biomed. Eng.*, vol. 17, no. 4, pp. 359–411, Jan. 1989.
[30] P. M. H. Rack and D. R. Westbury, "The effects of length and stimulus rate on tension in the isometric cat soleus muscle," *J. Physiol.*, vol. 204, no. 2, pp. 443–460, Oct. 1969.
[31] R. I. Close, "Dynamic properties of mammalian skeletal muscles," *Physiol. Rev.*, vol. 52, no. 1, pp. 129–197, Jan. 1972.
[32] T. A. McMahon, *Muscles, Reflexes, and Locomotion*, Princeton, NJ, USA: Princeton Univ. Press, 1984.
[33] Q. Luo, C. M. Niu, and N. Lan, "Effect of fascicle length range on force generation of model-based biomimetic controller for tendon-driven prosthetic hand," in *Proc. IEEE 43rd Annu. Int. Conf. Eng. Med. Biol. Soc.*, 2021, pp. 5856–5859.
[34] K. E. Jones, A. F. de C. Hamilton, and D. M. Wolpert, "Sources of signal-dependent noise during isometric force production," *J. Neurophysiol.*, vol. 88, no. 3, pp. 1533–1544, Sep. 2002.
[35] F. A. Mussa-Ivaldi, N. Hogan, and E. Bizzi, "Neural, mechanical, and geometric factors subserving arm posture in humans," *J. Neurosci.*, vol. 5, no. 10, Oct. 1985, Art. no. 13.
[36] E. Perreault, R. Kirsch, and P. Crago, "Effects of voluntary force generation on the elastic components of endpoint stiffness," *Exp. Brain Res.*, vol. 141, no. 3, pp. 312–323, Dec. 2001.
[37] G. J. C. Ettema and P. A. Huijing, "Skeletal muscle stiffness in static and dynamic contractions," *J. Biomech.*, vol. 27, no. 11, pp. 1361–1368, Nov. 1994.
[38] R. R. Carter, P. E. Crago, and M. W. Keith, "Stiffness regulation by reflex action in the normal human hand," *J. Neurophysiol.*, vol. 64, no. 1, pp. 105–118, Jul. 1990.
[39] J. A. Hoffer and S. Andreassen, "Regulation of soleus muscle stiffness in premammillary cats: Intrinsic and reflex components," *J. Neurophysiol.*, vol. 45, no. 2, pp. 267–285, Feb. 1981.
[40] T. R. Nichols and J. C. Houk, "Improvement in linearity and regulation of stiffness that results from actions of stretch reflex," *J. Neurophysiol.*, vol. 39, no. 1, pp. 119–142, Jan. 1976.
[41] N. Hogan, "Impedance control: An approach to manipulation," in *Proc. Amer. Control Conf.*, 1984, pp. 304–313.
[42] G. C. Agarwal and C. L. Gottlieb, "Compliance of the human ankle joint," *J. Biomech. Eng.*, vol. 99, no. 3, pp. 166–170, Aug. 1977.
[43] G. I. Zahalak, *Modeling muscle mechanics (and energetics)," in multiple muscle systems: Biomechanics and movement organization*, J. M. Winters and S. L.-Y. Woo Eds., New York, NY, USA: Springer, 1990, pp. 1–23.
[44] A. Prochazka, "Proprioception: Clinical relevance and neurophysiology," *Curr. Opin. Physiol.*, vol. 23, May 2021, Art. no. 100440.
[45] L. - Q. Zhang and W. Z. Rymer, "Simultaneous and nonlinear identification of mechanical and reflex properties of human elbow joint muscles," *IEEE Trans. Biomed. Eng.*, vol. 44, no. 12, pp. 1192–1209, Dec. 1997.
[46] R. Okuno, M. Yoshida, and K. Akazawa, "Development of biomimetic prosthetic hand controlled by electromyogram," in *Proc. IEEE 4th Int. Workshop Adv. Motion Control*, 1996, pp. 103–108.
[47] A. G. Fel'Dman, "Functional tuning of the nervous system with control of movement or maintenance of a steady posture – III. Mechanographic analysis of the execution by man of the simplest motor tasks," *Biofizika*, vol. 11, no. 4, pp. 766–775, Jan. 1966.
[48] J. D. Cooke, "Dependence of human arm movements on limb mechanical properties," *Brain Res.*, vol. 165, no. 2, pp. 366–369, Apr. 1979.
[49] E. J. Perreault, P. E. Crago, and R. F. Kirsch, "Estimation of intrinsic and reflex contributions to muscle dynamics: A modeling study," *IEEE Trans. Biomed. Eng.*, vol. 47, no. 11, pp. 1413–1421, Nov. 2000.
[50] T. E. Milner and D. W. Franklin, "Characterization of multijoint finger stiffness: Dependence on finger posture and force direction," *IEEE Trans. Biomed. Eng.*, vol. 45, no. 11, pp. 1363–1375, Nov. 1998.
[51] R. Shadmehr, "A mathematical muscle model," In: in *Supplementary Documents for 'Computational Neurobiology of Reaching and Pointing'*, Cambridge, U.K.: MIT Press, 2005.
[52] E. M. Izhikevich, "Simple model of spiking neurons," *IEEE Trans. Neural Netw.*, vol. 14, no. 6, pp. 1569–1572, Nov. 2003.
[53] C. M. Niu, K. Jalaleddini, W. J. Sohn, J. Rocamora, T. D. Sanger, and F. J. Valero-Cuevas, "Neuromorphic meets neuromechanics, Part I: The methodology and implementation," *J. Neural Eng.*, vol. 14, no. 2, Apr. 2017, Art. no. 025001.
[54] W. Mugge, J. Schuurmans, A. C. Schouten, and F. C. T. van der Helm, "Sensory weighting of force and position feedback in human motor control tasks," *J. Neurosci.*, vol. 29, no. 17, pp. 5476–5482, Apr. 2009.
[55] N. Lan, C. M. Niu, M. Hao, C. - H. Chou, and C. Dai, "Achieving neural compatibility with human sensorimotor control in prosthetic and therapeutic devices," *IEEE Trans. Med. Robot. Bionics*, vol. 1, no. 3, pp. 122–134, Aug. 2019.
[56] T. Flash and F. Mussa-Ivaldi, "Human arm stiffness characteristics during the maintenance of posture," *Exp. Brain Res.*, vol. 82, no. 2, Oct. 1990, pp. 315–326.
[57] F. Hug, K. Tucker, J. - L. Gennisson, M. Tanter, and A. Nordez, "Elastography for muscle biomechanics: Toward the estimation of individual muscle force," *Exercise Sport Sci. Rev.*, vol. 43, no. 3, pp. 125–133, Jul. 2015.
[58] C. S. Cook and M. J. N. McDonagh, "Measurement of muscle and tendon stiffness in man," *Eur. J. Appl. Physiol.*, vol. 72, no. 4, pp. 380–382, Jul. 1996.
[59] E. Bizzi, N. Hogan, F. A. Mussa-Ivaldi, and S. Giszter, "Does the nervous system use equilibrium-point control to guide single and multiple joint movements?," *Behav. Brain Sci.*, vol. 15, no. 4, pp. 603–613, Dec. 1992.
[60] N. Lan and X. He, "Fusimotor control of spindle sensitivity regulates central and peripheral coding of joint angles," *Front. Comput. Neurosci.*, vol. 6, Aug. 2012, Art. no. 66.
[61] C. M. Niu, S. K. Nandyala, and T. D. Sanger, "Emulated muscle spindle and spiking afferents validates VLSI neuromorphic hardware as a testbed for sensorimotor function and disease," *Front. Comput. Neurosci.*, vol. 8, Dec. 2014, Art. no. 141.
[62] B. B. Edin and A. B. Vallbo, "Stretch sensitization of human muscle spindles," *J. Physiol.*, vol. 400, no. 1, pp. 101–111, May, 1988.

[63] K. E. Jones, J. Wessberg, and Å. B. Vallbo, "Directional tuning of human forearm muscle afferents during voluntary wrist movements," *J. Physiol.*, vol. 536, no. 2, pp. 635–647, 2001.
[64] S. S. Srinivasan et al., "Agonist-antagonist myoneural interface amputation preserves proprioceptive sensorimotor neurophysiology in lower limbs," *Sci. Transl. Med.*, vol. 12, no. 573, Dec. 2020, Art. no. eabc5926.
[65] A. K. Silverman and R. R. Neptune, "Muscle and prosthesis contributions to amputee walking mechanics: A modeling study," *J. Biomech.*, vol. 45, no. 13, pp. 2271–2278, Aug. 2012.
[66] D. K. Kumar, B. Jelfs, X. Sui, and S. P. Arjunan, "Prosthetic hand control: A multidisciplinary review to identify strengths, shortcomings, and the future," *Biomed. Signal Process. Control*, vol. 53, Aug. 2019, Art. no. 101588.
[67] F. Baldissera, H. Hultborn, and M. Illert, "Integration in spinal neuronal systems," in *Handbook of Physiology I: The Nervous System*, V. B. Brooks Ed., Bethesda, MD, USA: American Physiological Society, 1981.
[68] P. Cavallari, E. Fournier, R. Katz, K. Malmgren, E. Pierrot-Deseilligny, and M. Shindo, "Cutaneous facilitation of transmission in ib reflex pathways in the human upper limb," *Exp. Brain Res.*, vol. 60, no. 1, pp. 197–199, Sep. 1985.
[69] A. Xie, C. - H. Chou, Q. Luo, Z. Zhang, and N. Lan, "Antagonistic control of a cable-driven prosthetic hand with neuromorphic model of muscle reflex," in *Proc. IEEE 44th Annu. Int. Conf. Eng. Med. Biol. Soc.*, 2022, pp. 732–735.
[70] C. A. Moran, "Anatomy of the hand," *Phys. Ther.*, vol. 69, no. 12, pp. 1007–1013, Dec. 1989.
[71] E. Henneman, G. Somjen, and D. O. Carpenter, "Functional significance of cell size in spinal motoneurons," *J. Neurophysiol.*, vol. 28, no. 3, pp. 560–580, May 1965.
[72] Y. Li, C. - H. Chou, J. Zhang, Z. Zhang, M. Hao, and N. Lan, "A pilot study of multi-site simultaneous stimulation for tactile and opening information feedback in the prosthetic hand," in *Proc. IEEE/EMBS 10th Int. Conf. Neural Eng.*, 2021, pp. 187–190.
[73] F. D. Kerkhof, T. van Leeuwen, and E. E. Vereecke, "The digital human forearm and hand," *J. Anat.*, vol. 233, no. 5, pp. 557–566, Sep. 2018.